

1 **A suite of Early Eocene (~55 Ma) climate model boundary conditions**

2  
3  
4  
5  
6  
7  
8  
9  
10  
11  
12  
13  
14  
15  
16

Herold, N.<sup>1</sup>, Buzan, J.<sup>2</sup>, Seton, M.<sup>3</sup>, Goldner, A.<sup>2</sup>, Green, J.A.M.<sup>4</sup>, Müller, R.D.<sup>3</sup>, Markwick, P.<sup>5</sup>, Huber, M.<sup>1,6\*</sup>

<sup>1</sup> Earth Systems Research Center, Institute for Earth, Ocean and Space Sciences, University of New Hampshire, Durham NH, USA.

<sup>2</sup> Department of Earth, Atmosphere, Planetary and Space Sciences, Purdue University, West Lafayette IN, USA.

<sup>3</sup> EarthByte Group, School of Geosciences, University of Sydney, Sydney NSW, Australia.

<sup>4</sup> School of Ocean Sciences, Bangor University, Menai Bridge, UK.

<sup>5</sup> Getech, Leeds, LS8 2LJ, UK.

<sup>6</sup> Department of Earth Sciences, University of New Hampshire, Durham NH, USA.

\*Corresponding author: Matthew Huber

E-mail: [matthew.huber@unh.edu](mailto:matthew.huber@unh.edu)

17

18 **Abstract**

19 We describe a set of Early Eocene (~55 Ma) climate model boundary conditions  
20 constructed in a self-consistent reference frame and incorporating recent data and  
21 methodologies. Given the growing need for uniform experimental design within the  
22 Eocene climate modelling community and the challenges faced in simulating the  
23 prominent features of Eocene climate, we make publically available our datasets of  
24 Eocene topography, bathymetry, tidal dissipation, vegetation, aerosol distributions and  
25 river runoff. Major improvements in our boundary conditions over previous efforts  
26 include the implementation of the ANTscape paleotopography of Antarctica, more  
27 accurate representations of the Drake Passage and Tasman Gateway, as well as an  
28 approximation of sub grid cell topographic variability. Our boundary conditions also  
29 include for the first time modelled estimates of Eocene aerosol distributions and tidal  
30 dissipation, both consistent with our paleotopography and paleobathymetry. The  
31 resolution of our datasets is unprecedented and will facilitate high resolution climate  
32 simulations. In light of the inherent uncertainties involved in reconstructing global  
33 boundary conditions for past time periods these datasets should be considered one  
34 interpretation of the available data and users are encouraged to modify them according  
35 to their needs and interpretations. This paper marks the beginning of a process for  
36 reconstructing a set of accurate, open-access Eocene boundary conditions for use in  
37 climate models.

38 **Keywords: Eocene, climate modelling, paleotopography, paleobathymetry, tidal**  
39 **dissipation, vegetation, aerosols, river runoff.**

40 **FIGURE CAPTIONS:**

- 41 1. Eocene topography from a) Sewall et al. (2000) and b) Markwick (2007), c) our  
42 revised Early Eocene topography.
- 43 2. Estimating the standard deviation of sub grid cell elevations for the Eocene. a)  
44 ETOPO1 topography downscaled from its native 1'x1' resolution to 1°x1°. b)  
45 Standard deviation of 1'x1' elevations inside each 1°x1° grid cell. c) Standard  
46 deviations from panel b area-weight averaged into 100 m bins and plotted  
47 against corresponding elevation. Standard error for each bin is plotted. Dotted  
48 lines represent linear regressions between sea-level and 3000 m, and 3000m and  
49 5500 m. d) Linear regressions from panel c applied to Eocene topography (Fig.  
50 1c). See text for details.
- 51 3. 55 Ma a) seafloor age, b) basement depth, c) sediment thickness, d) final  
52 bathymetry and e) the error margin in our bathymetry based on age-uncertainty  
53 (values represent the range of uncertainty above and below the bathymetry  
54 shown in panel d). Black outlines indicate paleo shoreline.
- 55 4. a) ETOPO1 topography and bathymetry, b) new Eocene topography and  
56 bathymetry. Both at 1°x1° resolution.
- 57 5. a) Modern and b) Eocene simulated tidal dissipation (Green and Huber, 2013).
- 58 6. a) Pre-industrial and b) Eocene vegetation simulated by BIOME4. The 27 biomes  
59 simulated by BIOME4 have been consolidated into 10 mega biomes following  
60 Harrison and Prentice (2003).
- 61 7. a) Pre-industrial and b) Eocene aerosol optical depth (unitless) simulated by the  
62 Community Atmosphere Model 4.
- 63 8. Eocene river runoff directions. Directions indicated by color.

64

65 **1. Introduction**

66 Growth of the paleoclimate modelling community has led to multiple independent  
67 efforts in modelling Eocene climate (Lunt et al., 2012). Several decades of paleoclimate  
68 modelling has further identified major limitations in the capabilities of climate models in  
69 capturing Earth's past greenhouse climates (Huber, 2012). The growth in research  
70 groups modelling Eocene climate as well as the challenges faced by the community in  
71 capturing pertinent aspects of this period make it desirable to distribute the boundary  
72 condition datasets used in published research. This serves two purposes: 1) that effort is  
73 not needlessly duplicated between research groups. The construction of boundary  
74 condition datasets for global climate models takes considerable effort and expertise.  
75 Thus, unless scientific disagreement exists, the process need only be conducted once; 2)  
76 that inter-model differences result only from variations in internal model assumptions  
77 and computational infrastructure. By holding boundary conditions fixed this enables a  
78 greater level of scientific understanding of the reasons for differences and commonalities  
79 between different groups' efforts. This was the impetus for the Paleoclimate Modelling  
80 Intercomparison Project (Braconnot et al., 2012), which assesses inter-model variation  
81 in Quaternary climate simulations and for which a consistent set of boundary conditions  
82 are openly available. Initiatives such as this have successfully fostered collaborations  
83 between research groups and provide a baseline for those wishing to conduct Quaternary  
84 climate simulations.

85 An ensemble of opportunity assembled in an ad hoc fashion - designated the  
86 Eocene Modelling Intercomparison Project (EoMIP) - has already been conducted using  
87 climate simulations described in studies published over the past several years (Lunt et  
88 al., 2012). Consequently, each model in this intercomparison differed at least partially  
89 with respect to their prescribed boundary condition forcing. In the spirit of encouraging  
90 data consistency within the Eocene climate modelling community we herein document a  
91 set of openly available and self-consistent climate model boundary conditions for the  
92 Early Eocene (~55 Ma). While their intended application is in climate modelling, the  
93 broadening domain of geoscientific models may see them applied in a variety of  
94 numerical frameworks (e.g. section 4). Specifically, this paper describes a newly updated  
95 Eocene topography, a necessary boundary condition for reconstructing past climates and  
96 one with a long history of inquiry in paleoclimate modelling (Donn and Shaw, 1977;  
97 Barron et al., 1981). An accompanying dataset of variation in sub grid cell scale Eocene  
98 elevations is also provided. We include a reconstructed Eocene bathymetry, which  
99 captures an unprecedented level of detail needed to meet the growing need for  
100 reconstructing regional Eocene oceanography (e.g. Hollis et al., 2012). The first estimate  
101 of Eocene tidal dissipation (Green and Huber, 2013) is also made available,  
102 complementing this recent addition to global climate models' suite of inputs and which  
103 may have particular relevance to Eocene climate and oceanography (Lyle, 1997). Eocene  
104 vegetation simulated by an offline dynamic vegetation model is also discussed and  
105 provided. Simulated Eocene aerosol distributions are provided - again taking advantage  
106 of this recent addition to atmospheric models' prognostic capabilities - to account for the  
107 direct effects of Eocene dust, sea salt, sulphate, and organic and black carbon. Finally,  
108 river runoff directions are provided based on the gradient of Eocene topography. All of  
109 our datasets, with the exception of aerosol distributions, are made available at 1°x1° to  
110 facilitate high resolution global and regional simulations.

111 Previous efforts have been made to assemble self-consistent Eocene boundary  
112 conditions (Sewall et al., 2000; Bice et al., 1998) and provide motivation for our work  
113 here. While our boundary conditions incorporate more recent data and methodologies  
114 than most of those used previously, there are many aspects of Eocene tectonics and  
115 climate that remain uncertain or controversial. Thus in many regions our boundary  
116 conditions merely reflect one interpretation of the available data and may conflict with  
117 alternate interpretations (e.g. elevation of the North American Cordillera). Our aim here  
118 is not to propose a 'correct' set of Eocene boundary conditions but to provide boundary  
119 conditions that can enable broader participation by the Eocene climate modelling  
120 community as well as greater transparency and reproducibility among groups.  
121 Researchers are encouraged to change these datasets based on their own data and  
122 interpretations.

## 123 **2. Topography**

### 124 *2.1 Background and base dataset*

125 The paleogeographic maps first used in climate modelling (Barron, 1980; Donn  
126 and Shaw, 1977) were semi-global in extent and were derived in large by Vinogradov et  
127 al. (1967) and Phillips and Forsyth (1972). However, the first global Eocene  
128 paleogeographic map applied to a climate model (Barron, 1985) was based on the work  
129 of Fred Ziegler and his colleagues at the University of Chicago, who had reconstructed a  
130 suite of Mesozoic to Cenozoic paleotopographies (Ziegler et al., 1982). These  
131 paleotopographies were built upon and succeeded by Christopher Scotese in the  
132 Paleomap Project (Scotese and Golonka, 1992), which was adopted by contemporary  
133 modelling efforts (Sloan and Rea, 1996; Sloan, 1994). Almost a decade later, Sewall et  
134 al. (2000) published a new global Eocene topography incorporating the latest regional  
135 tectonic data (Fig. 1a). For over a decade this dataset has remained, without update, a  
136 highly utilized topography for Eocene climate modelling (Huber and Caballero, 2011;  
137 Winguth et al., 2009; Huber et al., 2003; Shellito et al., 2009; DeConto et al., 2012),  
138 and thus a dataset incorporating more recent scholarship is overdue.

139 For both our Eocene topography and bathymetry we utilize base datasets that  
140 have been previously created. Here we adapt the Early Eocene paleotopographic map  
141 from Markwick (2007) (Fig. 1b). This map comes from a suite of Cretaceous to modern  
142 paleotopographies which – similar to the Paleomap project (Scotese and Golonka, 1992) –  
143 has its origins in the Paleogeographic Atlas Project at the University of Chicago (Ziegler  
144 et al., 1982). These maps have been augmented with more recent faunal, floral and  
145 lithological data and use a more recent rotation model (Rowley 1995 unpublished). The  
146 primary method used to derive this Eocene topography is based on that described by  
147 Ziegler et al. (1985) and further documented by Markwick (2007), in which contour  
148 intervals of 1000 m or less are estimated by comparing past tectonic regimes to their  
149 present day analogues. Subsequent to this adjustments to the paleo shoreline are made  
150 based on known Eocene biogeography (see fig. 39 Markwick, 2007 for a map of known  
151 records). Thus, the paleotopographic map of Markwick (2007) consists of a potential  
152 range of elevations for each grid cell, instead of an explicit value. A significant benefit of  
153 this method over others (e.g. Sewall et al., 2000) is obviation of the need for explicit  
154 paleo-elevation estimates - which are scarce for most time periods and regions - while  
155 providing an approximate yet quantitative description of topography over a wide area of  
156 the Earth. The obvious limitation, however, is the lack of precision and topographic detail

157 away from contour lines, which becomes significant in continental interiors where large  
158 anomalous plateaus appear (Fig. 1b).

159 Climate models require explicit and globally gridded elevation data so a  
160 conversion from the vector-based Geographic Information Systems approach underlying  
161 the topography of Markwick (2007) to a discrete digital elevation model was necessary.  
162 More importantly, detail in regions bounded by contour intervals was needed for which  
163 we applied a tension spline using the contour lines and sea-level as tie points. This  
164 creates continuous discrete elevations at all locations. In order to provide plausible peak  
165 elevations and gradients along known mountain ranges (e.g. the North American and  
166 Andean Cordilleras) artificial tie points were added by inserting mountain spines in these  
167 areas. The process of interpolation was performed using the `cssgrid` function (Cubic  
168 Spline Sphere Gridder) from the National Center for Atmospheric Research (NCAR)  
169 Command Language (UCAR/NCAR/CISL/VETS, 2013) and a constant tension factor of  
170 10, which provides a more linear interpolation between tie points as opposed to a pure  
171 cubic spline. This latter choice affects the roughness of the areas we interpolate between  
172 contour intervals.

## 173 *2.2 Topographic revisions*

174 Adjustments were made to conform the topography of Markwick (2007) to more  
175 recent or broadly accepted regional paleogeographic reconstructions. For Antarctica we  
176 adopt the ANTscape “maximum” topographic reconstruction (Wilson et al., 2012) which  
177 incorporates, among other improvements, a more elevated West Antarctic bedrock than  
178 previous reconstructions have recognised (c.f. Fig. 1a and c). This ANTscape  
179 reconstruction is specifically for the Eocene-Oligocene boundary (~34 Ma). However, it is  
180 significantly closer to the Early Eocene than isostatically relaxed modern day bedrock  
181 (DeConto and Pollard, 2003; Pollard and DeConto, 2005). Our choice of the maximum  
182 reconstruction by Wilson et al. (2012) is also compensated by the fact that the crust in  
183 the Early Eocene was younger than at 34 Ma and that the interpolation required to adapt  
184 our topography to a given climate model inherently smooths high and complex relief.  
185 The resolution and scholarship of this reconstruction is also unprecedented, and given  
186 that no substantial continental ice existed between the Early Eocene and Eocene-  
187 Oligocene transition (Cramer et al., 2011), uncertainty in the application of this dataset  
188 only arises from regional tectonics and not emplacement of thick ice-sheets. Future  
189 ANTscape reconstructions will include the Early Eocene and may form a part of revisions  
190 to the global topography presented here (<http://www.antscape.org/>).

191 While our dataset provides global coverage of land elevation there are several  
192 regions which suffer from large topographic uncertainty and which we highlight here.  
193 The southern margin of Eurasia (the proto-Himalayas) is one such area. Prior to India’s  
194 collision with Eurasia, between 55 and 45 Ma, geological evidence suggests Eurasia’s  
195 southern margin may have been up to 4 km high (Molnar et al., 2010 and references  
196 therein). However, recent thermochronologic and cosmogenic nuclide data indicate  
197 relatively low relief persisted prior to collision (Hetzl et al., 2011). We choose to leave  
198 our dataset as provided by Markwick (2007), with a peak elevation of 1,500 m, which  
199 represents an intermediate solution to these competing uplift histories. This is a region  
200 where researchers with new data or interpretations may wish to make changes.

201 The uplift history of North American Cordillera is also subject to debate.  
202 Numerous paleoaltimetry measurements based on oxygen isotope geochemistry suggest

203 that western North America was relatively high, on the order of 3 – 4 km, since the early  
204 Cenozoic (e.g. Mix et al., 2011). However, paleobotanical evidence suggests elevations  
205 were closer to 2 km (Wolfe et al., 1998) and it is known that atmospheric dynamics  
206 upwind of mountain ranges can significantly bias oxygen isotope records toward higher  
207 estimates of elevation (Galewsky, 2009). Thus we choose to constrain the maximum  
208 elevation of this region to the lower end of estimates, approximately 2,500 m (Fig. 1c).

209 Despite the uncertainties in our reconstructed topography, there are several  
210 substantial improvements over the reconstruction of Sewall et al. (2000). In addition to  
211 the changes discussed above, our topography incorporates a more realistic extent of the  
212 Mississippi Embayment, reducing its area in accordance with marine carbonate, coal and  
213 peat distributions (Sessa et al., 2012; Markwick, 2007) (Fig. 1). The ANTscape Antarctic  
214 topography is also substantially more accurate than that of Sewall et al. (2000), which  
215 had an erroneously small continental area. The width of the Drake Passage is also  
216 reduced in our reconstruction to be more in accordance with data which imply an  
217 extremely nascent – i.e. oceanographically closed – gateway in the Early Eocene (Barker  
218 et al., 2007; Lawver et al., 2011; Livermore et al., 2007). Additional improvements  
219 include paleogeographical adjustments to Australia (Langford, 2001) and Europe  
220 (Iakovleva et al., 2001; Golonka, 2011; Torsvik et al., 2002). Our final Eocene  
221 topography is shown in figure 1c.

### 222 *2.3 Representation of sub grid cell topographic variability*

223 Numerous details at the sub grid cell scale have important effects on resolvable  
224 processes in global atmospheric models and thus require parameterisation. An important  
225 detail is the variation of topography within each grid cell, which allows models to  
226 parameterize atmospheric gravity waves based on surface roughness. Global  
227 atmospheric circulation models are sensitive to the parameterized wave drag and to their  
228 waves. These waves are important for the atmosphere's momentum balance, jet stream  
229 strength and the vertical transport of tracers, such as H<sub>2</sub>O. In modern simulations the  
230 variability of sub grid cell scale topography is represented by the standard deviation of  
231 elevations within each model grid cell. For example, the variation of topography in a  
232 1°x1° model grid cell is calculated from the standard deviation of all elevations within  
233 the 1°x1° domain using a 1'x1' dataset (e.g. ETOPO1 (Amante and Eakin, 2009)).  
234 However, for past time periods knowledge of surface elevation at such a high resolution  
235 is impossible. To overcome this lack of information and provide an estimate of the  
236 Eocene variability of sub grid cell topography we use an empirical relationship between  
237 modern elevation and the standard deviation of sub grid cell scale topography, derived  
238 from the ETOPO1 dataset (Amante and Eakin, 2009). A script that performs this task on  
239 a given topographic dataset is provided in the electronic supplement.

240 In figure 2 we illustrate this process on our 1°x1° Eocene topography. Firstly, the  
241 modern ETOPO1 topography is regridded from its native 1'x1' resolution to 1°x1° (Fig.  
242 2a), then, within each 1°x1° grid cell the standard deviation of elevations in the original  
243 ETOPO1 dataset are calculated (Fig. 2b). The Greenland and Antarctic ice-sheets are  
244 replaced with the appropriate bedrock topography given the smoothness of ice compared  
245 to continental crust. Secondly, an array of 100 m bins are created from 0 m to 5,500 m  
246 – representing the range of modern elevations – and the area-weighted average of the  
247 standard deviations of the grid cells that fall within each bin (calculated in the previous  
248 step) are calculated, resulting in an array of 55 values (Fig. 2c). Lastly, given the clear  
249 monotonic relation between height and standard deviation between sea-level and

250 approximately 3000 m, and between 3000 m and 5500 m, separate linear regressions  
251 are calculated for these intervals (Fig. 2c) to assign estimates of Eocene variability in sub  
252 grid cell topography to each grid cell (Fig. 2d). Given that the maximum elevation in our  
253 Eocene topography is less than 3000 m (Fig. 1c) only the first linear regression is  
254 applicable here.

255 Figure 2c shows a peak in standard deviations of approximately 800 m at  
256 elevations between 2,500 m and 3,500 m. This corresponds to the “Andean-type”  
257 environments identified by Ziegler (1985) such as the boundaries of the Tibetan Plateau  
258 and Andean Cordillera (Fig. 2b). This broad peak remains regardless of the resolution we  
259 downscale ETOPO1 to, though its magnitude and width decreases with increasing  
260 resolution. Combined with an adequately derived atmospheric lapse rate, this dataset of  
261 sub grid cell scale topographic variability may be used to constrain uncertainty in  
262 simulated surface temperatures which result from differences in the paleo elevation of a  
263 proxy record’s site and the elevation resolved in a given climate model (e.g. Huber and  
264 Caballero, 2011; Sewall et al., 2000; Sewall and Sloan, 2006).

### 265 **3. Bathymetry**

#### 266 *3.1 Background and base dataset*

267 The first bathymetric maps used for Eocene ocean modelling constituted bowl-like  
268 basins in which the oceanic crust was treated primarily as abyssal plain (Barron and  
269 Peterson, 1991). The choice of a relatively flat bathymetry, although dictated to some  
270 extent by model resolution and available geological data, was informed by the lack of  
271 large scale oceanic responses to bathymetric details (Barron and Peterson, 1990).  
272 However, this result was misleading due to the lack of treatment of crucial oceanic  
273 processes in models of that generation (e.g. see section 4). The most recent Eocene  
274 bathymetric datasets included the locations of mid-ocean ridges and shelf slope  
275 hypsometry (Bice et al., 1998; Huber et al., 2003). However, given that the highest level  
276 of detail in these datasets consist of only six depth classes and  $\sim 3^\circ \times 1.5^\circ$  horizontal  
277 resolution, substantial gains are to be made by employing new methodologies and higher  
278 resolution base datasets to reconstruct Eocene bathymetry.

279 The base dataset for our bathymetry is formed from the global 55 Ma bathymetry  
280 of Müller et al. (2008b), which is part of a suite of paleobathymetric maps reconstructed  
281 from 140 Ma to the present. Like previous efforts the foundation of this bathymetry is  
282 the application of an age-depth relationship to reconstructed seafloor spreading  
283 isochrons. As lithospheric crust ages and cools on its path away from the mid-ocean  
284 ridge, thinning occurs (Fig. 3a and b). In constructing our Eocene bathymetry the age-  
285 depth relationship derived by Stein and Stein (1992) was applied to reconstructed 55 Ma  
286 seafloor ages;

$$287 \quad \text{If } t < 20 \text{ Ma; } d(t) = 2600 + 365t^{1/2}$$

$$288 \quad \text{If } t \geq 20 \text{ Ma; } d(t) = 5651 - 2473\exp(-0.0278t)$$

289 Where  $d$  is the basement depth in meters and  $t$  is time in Myrs. Several age-  
290 depth relationships have been previously tested to determine the best match to modern  
291 bathymetry, with Stein and Stein (1992) showing the least bias (Müller et al., 2008b).  
292 To accommodate regions where Eocene crust is not available at present (due to the  
293 subsequent subduction of oceanic crust) symmetric mid-ocean ridge spreading was

294 assumed and seafloor spreading isochrons from the conjugate plate applied. In regions  
295 where no data was available from the conjugate plate interpolation was applied between  
296 available isochrons and the adjacent plate margin (Müller et al., 2008a; Müller et al.,  
297 2008b).

298 On tectonic time scales (Myrs) the development of Large Igneous Provinces (LIPs)  
299 can have significant impacts on global sea-level (Müller et al., 2008b) and ocean  
300 circulation (Lawver et al., 2011), thus LIPs form an important component of our Eocene  
301 bathymetry. These bathymetric features are reconstructed by applying modern LIP  
302 outlines and estimating paleo LIP height following Schubert and Sandwell (1989).  
303 Additionally, given that certain regions of the modern ocean are covered by up to several  
304 kilometres of sediment (Whittaker et al., 2013) reconstructed sediment thicknesses also  
305 represent an important component of our reconstructed paleobathymetry. Based on an  
306 empirical relationship with age and latitude (polar latitudes generally having larger river  
307 runoff and tropical latitudes subject to high marine productivity), an age-latitude  
308 relationship was applied (Müller et al., 2008b supplementary material) to reconstruct  
309 Eocene sediment thickness (Fig. 3c).

### 310 *3.2 Bathymetric revisions*

311 While the methodology adopted from Müller et al. (2008b) represents a  
312 substantial improvement over previous bathymetric maps, it is by design a generic  
313 process used to reconstruct bathymetry over the past 140 Myrs. Therefore discrepancies  
314 exist in some regions where paleoceanographic data have been recovered. Particularly,  
315 the depths of certain LIPs may be verified against known depth habitats of foraminifera  
316 recovered from deep-sea cores. Such a verification was carried out here using Deep Sea  
317 Drilling Project and Ocean Drilling Project records. Based on these records the depth of  
318 the Madagascar Ridge (Schlich, 1974), Mascarene Ridge (Backman et al., 1988; Fisher  
319 et al., 1974; Vincent et al., 1974), Shatsky Rise, Ontong Java Plateau (Barrera, 1993),  
320 Kerguelen Plateau (Mackensen, 1992), Walvis Ridge (Zachos et al., 2005; Fuetterer,  
321 1984) and the Rio Grande Rise (Perch-Nielsen, 1977) were adjusted.

322 Reconstructing the tectonic history of ocean gateways is critical in explaining past  
323 ocean circulation (Scher and Martin, 2006; Hill et al., 2013), faunal migration patterns  
324 (Dalziel et al., 2013a) and potentially global climate change (Barker and Thomas, 2004).  
325 The Drake Passage and Tasman gateway are of particular significance given their  
326 opening was a requirement for development of the Antarctic Circumpolar Current, the  
327 largest ocean current in the world (~130 Sv) and the only current to be circum global  
328 (Barker and Thomas, 2004). Unfortunately, the Drake Passage suffers from poor age  
329 constraints due to the tectonically complex Scotia arc region and estimates of its opening  
330 range from the middle Eocene to late Miocene (c.f. Dalziel et al., 2013b; Scher and  
331 Martin, 2006). As our bathymetry aims to represent the Early Eocene we prescribe an  
332 oceanographically closed Drake Passage, constraining its depth to less than 100 m.  
333 Multiple paleoceanographic and tectonic records indicate that the Tasman gateway did  
334 not open to deep flow until the late Eocene (Sticklely et al., 2004), although when a  
335 shallow opening appeared is debatable. Our reconstruction of tectonic plate positions as  
336 well as the location of Tasmania suggests a shallow epi-continental sea may have  
337 existed and thus we prescribe a depth of 30 m or less in the Tasman gateway. Finally,  
338 no data is available for the bathymetry of inland seas or continental shelves in our base  
339 datasets and thus we derive their depths by assuming a maximum depth of 50 m for  
340 inland seas and using a Poisson equation solver to interpolate intermediate values for



341 both areas. Figure 3d shows our final Eocene bathymetry. The uncertainty in this  
342 bathymetry is shown in Figure 3e as a function of age uncertainty, with largest values in  
343 the southeast and northwest Pacific Ocean (Figure 3a).

### 344 *3.3 Consistent plate rotations*

345 The plate rotation model used to construct our paleobathymetry differs from that  
346 used for our Eocene topography (section 2). To maintain a consistent reference frame  
347 between the two datasets we re-rotate our Eocene topography using the plate rotation  
348 model of Müller et al. (2008b). This was achieved by changing the reference plate  
349 (Africa) location from that determined by Ziegler to that determined by Müller et al.  
350 (2008b), resulting in a relative shift of the other continents. Refinements to the location  
351 of some continental blocks were made to improve the match between the locations of  
352 continental crust in our bathymetry and topography. These steps were largely achieved  
353 using the open source software packages GPlates (<http://www.gplates.org/>), for  
354 digitizing polygons, and Generic Mapping Tools (<http://gmt.soest.hawaii.edu/>) for  
355 manual corrections. Deep integration of plate rotation software with open access  
356 paleontology databases has the potential to streamline future paleogeographic  
357 reconstructions (e.g. Wright et al., 2013). The final merged Eocene topography and  
358 bathymetry is shown in figure 4 alongside ETOPO1.

## 359 **4. Tidal dissipation**

360 The importance of tidal dissipation in the ocean's general circulation stems from  
361 the fact that diapycnal (i.e. vertical) mixing is greatly affected by the tide's interaction  
362 with bathymetry. Large increases in diapycnal mixing are observed above regions of  
363 rough topography (e.g. Polzin et al., 1997) and are primarily a result of breaking tidally  
364 induced internal waves (Garrett and Kunze, 2007; Jayne et al., 2004). Tidal models have  
365 been used to predict the amount of tidal energy dissipated in the oceans and to better  
366 constrain vertical mixing profiles incorporated in ocean general circulation models (e.g.  
367 Simmons et al., 2004). Such experiments have demonstrated that tidal energy  
368 considerations significantly reduce the discrepancy between simulated and observed  
369 modern ocean heat transport (Simmons et al., 2004) and provides motivation for  
370 explicitly including tidal dissipation in past climate simulations (e.g. Green and Huber,  
371 2013; Egbert et al., 2004).

372 New atmosphere-ocean general circulation models are beginning to incorporate  
373 tidal dissipation (e.g. the Community Earth System Model; CESM (Gent et al., 2011)).  
374 Green and Huber (2013) applied a tidal model using the bathymetry described in section  
375 3 and showed that, while total Eocene tidal dissipation was weaker than present, a larger  
376 amount of tidal energy was dissipated in the deep ocean, especially in the deep Pacific.  
377 The vertical diffusivities associated with these results are significantly larger than  
378 present, supporting arguments that enhanced vertical mixing in the Eocene oceans helps  
379 to explain the low equator to pole temperature gradient inferred from geological records  
380 (e.g. Lyle, 1997), but that have hitherto been difficult to reproduce in models (Lunt et  
381 al., 2012).

382 We distribute the dataset from Green and Huber (2013) here as a map of energy  
383 dissipated per unit area (Fig. 5). Models such as the National Center for Atmospheric  
384 Research CESM can utilize this dataset to drive their tidal mixing schemes. While this  
385 work represents a coarse first attempt at deriving Eocene tidal dissipation, to our

386 knowledge no similar effort has been made and thus this dataset provides a baseline for  
387 groups who do not have access to the tools required for deriving this boundary condition.  
388 However, given the infancy of this application to deep time paleoclimate it is likely that  
389 such a dataset will be improved upon quickly.

## 390 **5. Vegetation**

391 Climate models have long shown substantial global and regional climatic  
392 responses to vegetation change (Otto-Bliesner and Upchurch, 1997; Dutton and Barron,  
393 1997), though newer models indicate a weaker sensitivity (Henrot et al., 2010; Micheels  
394 et al., 2007). A series of Tertiary vegetation maps based on paleofloral records (Wolfe,  
395 1985) formed the foundation of many early paleoclimate simulations that explicitly  
396 included a paleovegetation boundary condition (e.g. Sloan and Rea, 1996; Dutton and  
397 Barron, 1997). Subsequently, Sewall et al. (2000) developed a new Eocene vegetation  
398 distribution taking into account more recent data and the effects of a low equator-to-pole  
399 temperature gradient. Like their Eocene topography, the vegetation reconstruction of  
400 Sewall et al. (2000) has remained highly utilized by the Eocene climate modelling  
401 community (e.g. Huber et al., 2003; Liu et al., 2009; Roberts et al., 2009; Huber and  
402 Caballero, 2011; Shellito et al., 2003).

403 We choose to reconstruct Early Eocene vegetation using the offline dynamic  
404 vegetation model BIOME4 (Kaplan et al., 2003). For input into BIOME4 we use  
405 temperature, precipitation and cloud cover from a CESM simulation forced with the  
406 Eocene topography and bathymetry described in sections 2 and 3, respectively, and an  
407 atmospheric CO<sub>2</sub> concentration of 2240 ppmv, a concentration which has been found to  
408 approximately reproduce Eocene temperatures (Huber and Caballero, 2011). This CESM  
409 simulation was integrated for 250 years and initialized with output from a previous CESM  
410 simulation that was integrated for over 3,000 years (this latter simulation was forced  
411 with the boundary conditions of Sewall et al. (2000) for topography and vegetation, and  
412 Huber et al. (2003) for bathymetry, mixed-layer ocean simulations of which are  
413 described by Goldner et al. (2013)). The BIOME4 was forced with a CO<sub>2</sub> concentration of  
414 1120 ppmv since higher concentrations resulted in large scale reductions in tropical  
415 forest. While this is not consistent with the CO<sub>2</sub> forcing of the driving climatology we are  
416 here only interested in deriving a vegetation distribution that is feasibly 'Eocene' in  
417 character. Figure 6a and b shows the simulated pre-industrial and Eocene distributions of  
418 biomes, respectively. For ease of comparison we show these biome maps simplified from  
419 the 27 biomes simulated by BIOME4 to 10 mega biomes after Harrison and Prentice  
420 (2003). Our BIOME4 simulated vegetation compares well with vegetation inferred from  
421 Paleocene and Eocene palynoflora (Utescher and Mosbrugger, 2007; Morley, 2007) and  
422 are consistent with geological indicators of climate (Crowley, 2012). One apparent bias is  
423 an abundance of relatively dry vegetation in northern South America in BIOME4 (cf.  
424 Morley, 2007). However, there remains a distinct lack of records for validation from large  
425 regions of South Africa and Siberia. We also note that 'grass' did not exist at the biome  
426 level in the Eocene (Strömberg, 2011), and thus the 'Grassland and dry shrubland'  
427 biome presented in Figure 6 should be interpreted as shrubland only. Our vegetation  
428 reconstruction reflects our simulated Eocene climate and is therefore less zonal than  
429 previous reconstructions (Sewall et al., 2000) and is consistent with our Eocene  
430 topography.

431 The utilisation of a single climate simulation to drive BIOME4 inherently results in  
432 a vegetation distribution that encompasses the biases of our climate model. While

433 utilisation of ensemble climate model data (Lunt et al., 2012) would attenuate individual  
434 model biases such datasets would deteriorate the representation of our new topography  
435 in the simulated vegetation. For example, many of the models evaluated in EoMIP were  
436 forced with the topography of Sewall et al. (2000) in which certain continents were  
437 several degrees of latitude or longitude offset from our new topography. Furthermore,  
438 most of these simulations were run at a substantially lower resolution than done here.  
439 Thus, utilising such datasets would result in mountainous vegetation – for example over  
440 the North American cordillera – not completely corresponding to the location of mountain  
441 ranges in our topography. Such an issue may be improved over time as more  
442 simulations are conducted with the topographic boundary condition presented here.

443 Due to the significant differences between modern and Eocene topography (Fig.  
444 4), the anomaly method typically used for specifying input into the BIOME4 (Kaplan et  
445 al., 2003) was not possible and thus first order biases in our control CESM simulation are  
446 not taken into consideration. However, given that the CESM simulates modern land and  
447 sea-surface temperatures broadly consistent with observations (Gent et al., 2011) and  
448 that the biases in the modern CESM climate are small in comparison with the simulated  
449 change in climate for the Eocene (Huber and Caballero, 2011) we do not believe this to  
450 be a significant issue. Furthermore, while asynchronous coupling between our climate  
451 and vegetation models precludes the ability of the simulated vegetation to affect climate  
452 - as compared to synchronous coupling efforts (e.g. Shellito and Sloan, 2006a, b) - it  
453 benefits our results by not erroneously amplifying biases in our climate model (e.g.  
454 Wohlfahrt et al., 2008).

## 455 **6. Aerosols**

456 Aerosols in Eocene climate simulations have previously been prescribed at pre-  
457 industrial levels or set to arbitrarily determined, globally uniform values. Aerosols  
458 constitute one of the largest uncertainties in radiative forcing under future anthropogenic  
459 greenhouse warming (Stocker et al., 2013) and may be important in resolving some long  
460 standing paleoclimate conundrums (Kump and Pollard, 2008). Insufficient proxies from  
461 the pre-Quaternary prevent the reconstruction of this boundary condition from geological  
462 records. However, the advent of aerosol prognostic capabilities in atmospheric models  
463 allows the paleo-distribution of various aerosol species to be simulated (Heavens et al.,  
464 2012). Here we again employ the NCAR CESM in a configuration that utilizes the newly  
465 implemented Bulk Aerosol Model, which is a component of the Community Atmosphere  
466 Model 4 (Neale and Co-authors, 2010). In this configuration the model explicitly  
467 simulates the monthly horizontal and vertical distribution of dust, sea salt, sulphate, and  
468 organic and black carbon aerosols consistent with our Eocene topography (Fig. 7). The  
469 Bulk Aerosol Model makes simplistic assumptions regarding the size distribution of  
470 aerosol species, compared to the more complicated Modal Aerosol Models. A detailed  
471 description of the steps involved in simulating the paleo-distribution of aerosols is  
472 provided by Heavens et al. (2012). Here we branch the same CESM simulation described  
473 in section 5 while also enabling the Bulk Aerosol Model.

474 Various aerosol species require the prescription of emission sources in the Bulk  
475 Aerosol Model and this is done in accordance with Heavens et al. (2012). One exception  
476 is that we do not specify any volcanic sources of SO<sub>2</sub> or SO<sub>4</sub>, given their small radiative  
477 effects and the uncertainty in the distribution of Eocene volcanoes. Another largely  
478 unconstrained yet climatically relevant emission source in the Bulk Aerosol Model is that  
479 of dust. In the Bulk Aerosol Model dust is emitted solely from the desert plant functional

480 type which in turn is determined from the prescribed vegetation dataset. It is generally  
481 understood that cooler climates promote more dust-laden atmospheres - due to  
482 increases in desertification, reduced soil moisture and stronger winds (Bar-Or et al.,  
483 2008). However, the degree to which global Eocene dust concentrations differed from  
484 typical glacial-interglacial variability is uncertain, though regional evidence exists for  
485 substantially weak dust fluxes in the early Cenozoic (Janecek and Rea, 1983). Here we  
486 have assumed that global Eocene dust loading was approximately three quarters that of  
487 the pre-industrial era. The sources of dust in our dataset (i.e. deserts) were manually  
488 distributed based loosely on the distribution of Early Eocene evaporites (Crowley, 2012),  
489 which itself follows the expected distribution of subtropical high pressure regions. Our  
490 chosen concentrations provide an Eocene dust loading intermediate to simulations which  
491 prescribe pre-industrial values (e.g. Heinemann et al., 2009; Lunt et al., 2010; Winguth  
492 et al., 2009) and those which eliminate the radiative effects of aerosols altogether  
493 (Huber and Caballero, 2011). The significant improvement in the approach taken here is  
494 that the distribution of aerosols is consistent with our Eocene topography, providing a  
495 realistic regional representation of their radiative forcing.

496 It is important to stress the large uncertainty in aerosol loading and distribution  
497 during past climates and that our simulated concentrations are likely highly model  
498 dependant. Furthermore, the aerosol datasets provided here are only adequate for  
499 models that do not include the indirect effects of aerosols. Models that include such  
500 effects may exhibit significant sensitivity to even slight changes in aerosol distribution  
501 and loading and we are not confident that the use of the datasets presented here, given  
502 the uncertainties involved, would be scientifically sound.

503 Finally, we note that the ability to prognose aerosol distributions in long climate  
504 simulations (available in the latest atmospheric models, though at significant  
505 computational cost) will obviate the need for prescribed aerosol concentrations while also  
506 accounting for their indirect effects. Such models will see the emission sources of various  
507 aerosol species (e.g. deserts, volcanoes, regions of high marine productivity) become an  
508 additional paleoclimate model boundary condition.

## 509 **7. River transport**

510 River runoff in current generation climate models is important primarily for the  
511 redistribution of fresh water to the oceans and can have significant implications for deep  
512 water formation (e.g. Bice et al., 1997). Here we use the gradient of our Eocene  
513 topography to represent river runoff direction (Fig. 7). This dataset was created using  
514 scripts made available by the National Center for Atmospheric Research (Rosenbloom et  
515 al., 2011). Regions where vectors do not reach the ocean (i.e. internal basins) were  
516 manually corrected. Topographic gradient has been used to constrain river directions in  
517 the overwhelming majority of paleoclimate simulations to date. However, it is a crude  
518 method which we show here simply for completeness. Furthermore, the dataset provided  
519 (Fig. 7) is only illustrative as the regridding of our topography (Fig. 1) to a given climate  
520 model's resolution will require re-calculation of these river directions to account for  
521 changes in gradient. A more morphologically constrained river direction dataset (e.g.  
522 Markwick and Valdes, 2004) should be integrated into future revisions of our Eocene  
523 boundary conditions.

## 524 **8. Discussion and Future Work**

525 We describe an openly available and comprehensive set of Early Eocene climate  
526 model boundary conditions including topography, bathymetry, tidal dissipation,  
527 vegetation, aerosols and river transport. The resolution of most of these datasets is  
528 unprecedented and alleviates the undesirable step of downscaling lower resolution  
529 datasets to that of current generation climate models. This should lead to improvements  
530 in model-data comparison in regions of strong relief and facilitate high resolution global  
531 and regional climate simulations.

532 An important distinction between our tidal, vegetation, aerosol datasets, and our  
533 topography and bathymetry datasets, is that the former are model-derived and thus not  
534 directly based on measured physical quantities. The use of modelling frameworks for our  
535 tidal and aerosol boundary conditions is necessitated by the absence of any quantitative  
536 Eocene data. Our use of a model to derive Eocene vegetation was predicated on the  
537 model's ability to capture what is known about Eocene vegetation from paleobotanical  
538 records (model validation). As this is the case (see section 5) we can have an at least (or  
539 perhaps at best) satisfactory level of confidence that the model is not predicting  
540 unrealistic vegetation in regions where data is scarce. This eliminates the need for  
541 researchers to subjectively estimate vegetation for large swathes of land, though of  
542 course is directly affected by the climate biases of our driving climatology.

543 Despite the substantial improvements introduced in these boundary conditions,  
544 uncertainties in the data remain. These are most pertinent in the paleo-elevation of the  
545 North American Cordillera and proto-Himalayas, the geometry of the Drake Passage and  
546 Tasman Gateway, our modelled tidal dissipation and aerosol distributions and lastly our  
547 rudimentary representation of river runoff. These data- and model- based uncertainties  
548 provide a natural focus for future research in developing new methods of inquiry (or  
549 eliminating old ones) and in focusing efforts on data collection. Reconciling tectonic  
550 models and paleo-elevation proxies will be crucial for reducing paleotopographic  
551 uncertainty in revised versions of these boundary conditions. On the other hand,  
552 advances in modelling may substantially improve the reconstruction of tidal dissipation  
553 and aerosol distributions, though quantitative validation of either of these in the Eocene  
554 is next to impossible.

555 Finally, as important as the input into any model representing a real-world  
556 system is, an at least equal importance should be placed on the data against which such  
557 models are validated. Fortunately, recent compilations of terrestrial and marine data  
558 have already been conducted by Huber and Caballero (2011) and Lunt et al. (2012),  
559 respectively. We stress that the maintenance and public availability of such datasets  
560 provides the necessary yardstick against which to compare all models. Users are also  
561 able to rotate newly collected data to their 55 Ma position in the same reference frame  
562 used here via the open source software package GPLates (<http://www.gplates.org/>), thus  
563 ensuring consistency in georeferencing is maintained. A community effort to adopt  
564 consistent modelling methodologies and boundary conditions can accelerate growth in  
565 our understanding of Eocene climates and specifically help highlight the most pertinent  
566 shortcomings of the current generation of climate models in simulating extreme  
567 greenhouse warmth.

## 568 **9. Acknowledgements**

569 NH, JB, AG and MH are supported under *1049921-EAR: Collaborative Research:*  
570 *Improved Cenozoic paleoelevation estimates for the Sierra Nevada, California: Linking*

571 *geodynamics with atmospheric dynamics*. MS and RDM acknowledge support from  
572 Australian Research Council (ARC) grants DP0987713 and FL0992245, respectively. The  
573 tidal model simulations were funded by the Natural Environmental Research Council  
574 (grant NE/F014821/1) and the Climate Change Consortium for Wales (JAMG), and the  
575 National Science Foundation (grant 0927946-ATM to MH). The NCAR Command  
576 Language (NCL) was used to create our figures. NCL and Generic Mapping Tools were  
577 used for the manipulation of data.

## 578 **10. References**

- 579 Backman, J., Duncan, R. A., Peterson, L. C., Baker, P. A., Baxter, A. N., Boersma, A.,  
580 Cullen, J. L., Droxler, A. W., Fisk, M. R., Greenough, J. D., Hargraves, R. B.,  
581 Hempel, P., Hobart, M. A., Hurley, M. T., Johnson, D. A., Macdonald, A. H.,  
582 Mikkelsen, N., Okada, H., Rio, D., Robinson, S. G., Schneider, D., Swart, P. K.,  
583 Tatsumi, Y., Vandamme, D., Vilks, G., and Vincent, E.: Site 707, ODP Ocean  
584 Drilling Program, 1988.
- 585 Bar-Or, R., Erlick, C., and Gildor, H.: The role of dust in glacial–interglacial cycles,  
586 *Quaternary Science Reviews*, 27, 201-208,  
587 <http://dx.doi.org/10.1016/j.quascirev.2007.10.015>, 2008.
- 588 Barker, P. F., and Thomas, E.: Origin, signature and palaeoclimatic influence of the  
589 Antarctic Circumpolar Current, *Earth-Science Reviews*, 66, 143-162, 2004.
- 590 Barker, P. F., Filippelli, G. M., Florindo, F., Martin, E. E., and Scher, H. D.: Onset and role  
591 of the Antarctic Circumpolar Current, *Deep Sea Research Part II: Topical Studies*  
592 *in Oceanography*, 54, 2388-2398, <http://dx.doi.org/10.1016/j.dsr2.2007.07.028>,  
593 2007.
- 594 Barrera, E. B., Jack; Lohmann, Kyger C.: Strontium isotope and benthic foraminifer  
595 stable isotope results from Oligocene sediments at Site 803, ODP Ocean Drilling  
596 Program, 1993.
- 597 Barron, E. J.: *Paleogeography and Climate, 180 Million Years to the Present*, University  
598 of MIAMI, 1980.
- 599 Barron, E. J., Thompson, S. L., and Schneider, S. H.: An Ice-Free Cretaceous? Results  
600 from Climate Model Simulations, *Science*, 212, 501-508,  
601 10.1126/science.212.4494.501, 1981.
- 602 Barron, E. J.: Explanations of the Tertiary global cooling trend, *Palaeogeography,*  
603 *Palaeoclimatology, Palaeoecology*, 50, 45-61, 1985.
- 604 Barron, E. J., and Peterson, W. H.: Mid-Cretaceous ocean circulation: Results from model  
605 sensitivity studies, *Paleoceanography*, 5, 319-337, 10.1029/PA005i003p00319,  
606 1990.
- 607 Barron, E. J., and Peterson, W. H.: The Cenozoic ocean circulation based on ocean  
608 General Circulation Model results, *Palaeogeography, Palaeoclimatology,*  
609 *Palaeoecology*, 83, 1-28, 1991.
- 610 Bice, K. L., Barron, E. J., and Peterson, W. H.: Continental runoff and early Cenozoic  
611 bottom-water sources, *Geology*, 25, 951-954, 1997.
- 612 Bice, K. L., Barron, E. J., and Peterson, W. H.: Reconstruction of realistic early Eocene  
613 paleobathymetry and ocean GCM sensitivity to specified basin configuration,  
614 *Oxford Monographs on Geology and Geophysics*, 39, 227-247, 1998.
- 615 Braconnot, P., Harrison, S. P., Kageyama, M., Bartlein, P. J., Masson-Delmotte, V., Abe-  
616 Ouchi, A., Otto-Bliesner, B., and Zhao, Y.: Evaluation of climate models using  
617 palaeoclimatic data, *Nature Clim. Change*, 2, 417-424,  
618 [http://www.nature.com/nclimate/journal/v2/n6/abs/nclimate1456.html#supplem](http://www.nature.com/nclimate/journal/v2/n6/abs/nclimate1456.html#supplementary-information)  
619 [entary-information](http://www.nature.com/nclimate/journal/v2/n6/abs/nclimate1456.html#supplementary-information), 2012.
- 620 Cramer, B. S., Miller, K. G., Barrett, P. J., and Wright, J. D.: Late Cretaceous–Neogene  
621 trends in deep ocean temperature and continental ice volume: Reconciling  
622 records of benthic foraminiferal geochemistry ( $\delta^{18}\text{O}$  and Mg/Ca) with sea level  
623 history, *Journal of Geophysical Research: Oceans*, 116, C12023,  
624 10.1029/2011jc007255, 2011.

625 Crowley, C. W.: An atlas of Cenozoic climates, Masters of science in geology, The  
626 University of Texas, 2012.

627 Dalziel, I. W. D., Lawver, L. A., Norton, I. O., and Gahagan, L. M.: The Scotia Arc:  
628 Genesis, Evolution, Global Significance, Annual Review of Earth and Planetary  
629 Sciences, 41, 767-793, doi:10.1146/annurev-earth-050212-124155, 2013a.

630 Dalziel, I. W. D., Lawver, L. A., Pearce, J. A., Barker, P. F., Hastie, A. R., Barfod, D. N.,  
631 Schenke, H.-W., and Davis, M. B.: A potential barrier to deep Antarctic  
632 circumpolar flow until the late Miocene?, Geology, 10.1130/g34352.1, 2013b.

633 DeConto, R. M., and Pollard, D.: Rapid Cenozoic glaciation of Antarctica induced by  
634 declining atmospheric CO<sub>2</sub>, Nature, 421, 245-249, 2003.

635 DeConto, R. M., Galeotti, S., Pagani, M., Tracy, D., Schaefer, K., Zhang, T., Pollard, D.,  
636 and Beerling, D. J.: Past extreme warming events linked to massive carbon  
637 release from thawing permafrost, Nature, 484, 87-91,  
638 [http://www.nature.com/nature/journal/v484/n7392/abs/nature10929.html#suppl](http://www.nature.com/nature/journal/v484/n7392/abs/nature10929.html#supplementary-information)  
639 [ementary-information](http://www.nature.com/nature/journal/v484/n7392/abs/nature10929.html#supplementary-information), 2012.

640 Donn, W. L., and Shaw, D. M.: Model of climate evolution based on continental drift and  
641 polar wandering, Geological Society of America Bulletin, 88, 390-396,  
642 10.1130/0016-7606(1977)88<390:mocebo>2.0.co;2, 1977.

643 Dutton, J. F., and Barron, E. J.: Miocene to present vegetation changes; a possible piece  
644 of the Cenozoic cooling puzzle, Geology, 25, 39-41, 1997.

645 Egbert, G. D., Ray, R. D., and Bills, B. G.: Numerical modeling of the global semidiurnal  
646 tide in the present day and in the last glacial maximum, Journal of Geophysical  
647 Research: Oceans, 109, C03003, 10.1029/2003jc001973, 2004.

648 Fisher, R. L., Bunce, E. T., Cernock, P. J., Clegg, D. C., Cronan, D. S., Damiani, V. V.,  
649 Dmitriev, L. V., Kinsman, D. J., Roth, P. H., Thiede, J., and Vincent, E.: Site 237,  
650 DSDP Deep Sea Drilling Project, 1974.

651 Fuetterer, D. K.: Bioturbation and trace fossils in deep sea sediments of the Walvis  
652 Ridge, southeastern Atlantic, Leg 74, DSDP Deep Sea Drilling Project; IPOD  
653 International Phase of Ocean Drilling, 1984.

654 Galewsky, J.: Orographic precipitation isotopic ratios in stratified atmospheric flows:  
655 Implications for paleoelevation studies, Geology, 37, 791-794,  
656 10.1130/g30008a.1, 2009.

657 Garrett, C., and Kunze, E.: Internal Tide Generation in the Deep Ocean, Annual Review  
658 of Fluid Mechanics, 39, 57-87, doi:10.1146/annurev.fluid.39.050905.110227,  
659 2007.

660 Gent, P. R., Danabasoglu, G., Donner, L. J., Holland, M. M., Hunke, E. C., Jayne, S. R.,  
661 Lawrence, D. M., Neale, R. B., Rasch, P. J., Vertenstein, M., Worley, P. H., Yang,  
662 Z.-L., and Zhang, M.: The Community Climate System Model Version 4, Journal of  
663 Climate, 24, 4973-4991, 10.1175/2011jcli4083.1, 2011.

664 Goldner, A., Huber, M., and Caballero, R.: Does Antarctic glaciation cool the world?,  
665 Clim. Past, 9, 173-189, 10.5194/cp-9-173-2013, 2013.

666 Golonka, J.: Chapter 6 Phanerozoic palaeoenvironment and palaeolithofacies maps of the  
667 Arctic region, Geological Society, London, Memoirs, 35, 79-129, 10.1144/m35.6,  
668 2011.

669 Green, J. A. M., and Huber, M.: Tidal dissipation in the early Eocene and implications for  
670 ocean mixing, Geophysical Research Letters, 40, 2707-2713, 10.1002/grl.50510,  
671 2013.

672 Harrison, S. P., and Prentice, C. I.: Climate and CO<sub>2</sub> controls on global vegetation  
673 distribution at the last glacial maximum: Analysis based on palaeovegetation  
674 data, biome modelling and palaeoclimate simulations, Global Change Biology, 9,  
675 983-1004, 2003.

676 Heavens, N. G., Shields, C. A., and Mahowald, N. M.: A paleogeographic approach to  
677 aerosol prescription in simulations of deep time climate, Journal of Advances in  
678 Modeling Earth Systems, 4, M11002, 10.1029/2012ms000166, 2012.

679 Heinemann, M., Jungclaus, J. H., and Marotzke, J.: Warm Paleocene/Eocene climate as  
680 simulated in ECHAM5/MPI-OM, Clim. Past, 5, 785-802, 10.5194/cp-5-785-2009,  
681 2009.

682 Henrot, A. J., François, L., Favre, E., Butzin, M., Ouberdous, M., and Munhoven, G.:  
683 Effects of CO<sub>2</sub>, continental distribution, topography and vegetation changes on  
684 the climate at the Middle Miocene: a model study, *Clim. Past*, 6, 675-694,  
685 10.5194/cp-6-675-2010, 2010.

686 Hetzel, R., Dunkl, I., Haider, V., Strobl, M., von Eynatten, H., Ding, L., and Frei, D.:  
687 Penepain formation in southern Tibet predates the India-Asia collision and  
688 plateau uplift, *Geology*, 39, 983-986, 10.1130/g32069.1, 2011.

689 Hill, D. J., Haywood, A. M., Valdes, P. J., Francis, J. E., Lunt, D. J., Wade, B. S., and  
690 Bowman, V. C.: Paleogeographic controls on the onset of the Antarctic  
691 circumpolar current, *Geophysical Research Letters*, 2013GL057439,  
692 10.1002/grl.50941, 2013.

693 Hollis, C. J., Taylor, K. W. R., Handley, L., Pancost, R. D., Huber, M., Creech, J. B.,  
694 Hines, B. R., Crouch, E. M., Morgans, H. E. G., Crampton, J. S., Gibbs, S.,  
695 Pearson, P. N., and Zachos, J. C.: Early Paleogene temperature history of the  
696 Southwest Pacific Ocean: Reconciling proxies and models, *Earth and Planetary  
697 Science Letters*, 349-350, 53-66, 10.1016/j.epsl.2012.06.024, 2012.

698 Huber, M., and Caballero, R.: The early Eocene equable climate problem revisited, *Clim.  
699 Past*, 7, 603-633, 10.5194/cp-7-603-2011, 2011.

700 Huber, M.: Progress in greenhouse climate modelling, in: *Reconstructing Earth's Deep-  
701 Time Climate*, edited by: Linda Ivany, B. H., Paleontological Society, 2012.

702 Iakovleva, A. I., Brinkhuis, H., and Cavagnetto, C.: Late Palaeocene-Early Eocene  
703 dinoflagellate cysts from the Turgay Strait, Kazakhstan; correlations across  
704 ancient seaways, *Palaeogeography, Palaeoclimatology, Palaeoecology*, 172, 243-  
705 268, [http://dx.doi.org/10.1016/S0031-0182\(01\)00300-5](http://dx.doi.org/10.1016/S0031-0182(01)00300-5), 2001.

706 Janecek, T. R., and Rea, D. K.: Eolian deposition in the northeast Pacific Ocean:  
707 Cenozoic history of atmospheric circulation, *Geological Society of America  
708 Bulletin*, 94, 730-738, 10.1130/0016-7606(1983)94<730:editnp>2.0.co;2, 1983.

709 Jayne, S. R., St Laurent, L. C., and Gille, S. T.: Connections between ocean bottom  
710 topography and Earth's climate, 2004.

711 Kaplan, J. O., Bigelow, N. H., Prentice, I. C., Harrison, S. P., Bartlein, P. J., Christensen,  
712 T. R., Cramer, W., Matveyeva, N. V., McGuire, A. D., Murray, D. F., Razzhivin, V.  
713 Y., Smith, B., Walker, D. A., Anderson, P. M., Andreev, A. A., Brubaker, L. B.,  
714 Edwards, M. E., and Lozhkin, A. V.: Climate change and Arctic ecosystems: 2.  
715 Modeling, paleodata-model comparisons, and future projections, *J. Geophys.  
716 Res.*, 108, 8171, 10.1029/2002jd002559, 2003.

717 Kump, L. R., and Pollard, D.: Amplification of Cretaceous Warmth by Biological Cloud  
718 Feedbacks, *Science*, 320, 195-, 10.1126/science.1153883, 2008.

719 Lawver, L. A., Gahagan, L. M., and Dalziel, I. W. D. I. W. D.: A Different Look at  
720 Gateways: Drake Passage and Australia/Antarctica, in: *Tectonic, Climatic, and  
721 Cryospheric Evolution of the Antarctic Peninsula*, American Geophysical Union, 5-  
722 33, 2011.

723 Liu, Z., Pagani, M., Zinniker, D., DeConto, R., Huber, M., Brinkhuis, H., Shah, S. R.,  
724 Leckie, R. M., and Pearson, A.: Global Cooling During the Eocene-Oligocene  
725 Climate Transition, *Science*, 323, 1187-1190, 10.1126/science.1166368, 2009.

726 Livermore, R., Hillenbrand, C.-D., Meredith, M., and Eagles, G.: Drake Passage and  
727 Cenozoic climate: An open and shut case?, *Geochem. Geophys. Geosyst.*, 8,  
728 Q01005, 10.1029/2005gc001224, 2007.

729 Lunt, D. J., Valdes, P. J., Jones, T. D., Ridgwell, A., Haywood, A. M., Schmidt, D. N.,  
730 Marsh, R., and Maslin, M.: CO<sub>2</sub>-driven ocean circulation changes as an amplifier  
731 of Paleocene-Eocene thermal maximum hydrate destabilization, *Geology*, 38,  
732 875-878, 10.1130/g31184.1, 2010.

733 Lunt, D. J., Dunkley Jones, T., Heinemann, M., Huber, M., LeGrande, A., Winguth, A.,  
734 Loptson, C., Marotzke, J., Roberts, C. D., Tindall, J., Valdes, P., and Winguth, C.:  
735 A model-data comparison for a multi-model ensemble of early Eocene  
736 atmosphere-ocean simulations: EoMIP, *Clim. Past*, 8, 1717-1736, 10.5194/cp-8-  
737 1717-2012, 2012.



738 Lyle, M.: Could early Cenozoic thermohaline circulation have warmed the poles?,  
739 *Paleoceanography*, 12, 161-167, 1997.

740 Mackensen, A. B., William A.: Paleogene benthic foraminifers from the southern Indian  
741 Ocean (Kerguelen Plateau); biostratigraphy and paleoecology, ODP Ocean Drilling  
742 Program, 1992.

743 Markwick, P. J., and Valdes, P. J.: Palaeo-digital elevation models for use as boundary  
744 conditions in coupled ocean-atmosphere GCM experiments: a Maastrichtian (late  
745 Cretaceous) example, *Palaeogeography, Palaeoclimatology, Palaeoecology*, 213,  
746 37-63, 2004.

747 Markwick, P. J.: The palaeogeographic and palaeoclimatic significance of climate proxies  
748 for data-model comparisons, in: *Deep-Time Perspectives on Climate Change: Marrying the Signal from Computer Models and Biological Proxies.*, edited by:  
749 Williams, M., Haywood, A.M., Gregory, J. and Schmidt D.N., Geological Society  
750 Special Publication, 251-312, 2007.

751 Micheels, A., Bruch, A. A., Uhl, D., Utescher, T., and Mosbrugger, V.: A Late Miocene  
752 climate model simulation with ECHAM4/ML and its quantitative validation with  
753 terrestrial proxy data, *Palaeogeography, Palaeoclimatology, Palaeoecology*, 253,  
754 251-270, 2007.

755  
756 Mix, H. T., Mulch, A., Kent-Corson, M. L., and Chamberlain, C. P.: Cenozoic migration of  
757 topography in the North American Cordillera, *Geology*, 39, 87-90,  
758 10.1130/g31450.1, 2011.

759 Molnar, P., Boos, W. R., and Battisti, D. S.: Orographic Controls on Climate and  
760 Paleoclimate of Asia: Thermal and Mechanical Roles for the Tibetan Plateau,  
761 *Annual Review of Earth and Planetary Sciences*, 38, 77-102,  
762 doi:10.1146/annurev-earth-040809-152456, 2010.

763 Morley, R. J.: Cretaceous and Tertiary climate change and the past distribution of  
764 megathermal rainforests, in: *Tropical Rainforest Responses to Climatic Change*,  
765 Springer Praxis Books, Springer Berlin Heidelberg, 1-31, 2007.

766 Müller, R. D., Sdrolias, M., Gaina, C., and Roest, W. R.: Age, spreading rates, and  
767 spreading asymmetry of the world's ocean crust, *Geochem. Geophys. Geosyst.*,  
768 9, Q04006, 10.1029/2007gc001743, 2008a.

769 Müller, R. D., Sdrolias, M., Gaina, C., Steinberger, B., and Heine, C.: Long-Term Sea-  
770 Level Fluctuations Driven by Ocean Basin Dynamics, *Science*, 319, 1357-1362,  
771 2008b.

772 Neale, R. B., and Co-authors: Description of the NCAR Community Atmosphere Model  
773 (CAM 4.0) National Center for Atmospheric Research, 2010.

774 Otto-Bliesner, B. L., and Upchurch, G. R.: Vegetation-induced warming of high-latitude  
775 regions during the Late Cretaceous period, *Nature (London)*, 385, 804-807, 1997.

776 Perch-Nielsen, K. S., P. R.; Boersma, A.; Carlson, R. L.; Dinkelman, M. G.; Fodor, R. V.;  
777 Kumar, N.; McCoy, F.; Thiede, J.; Zimmerman, H. B.: Site 357; Rio Grande Rise,  
778 DSDP Deep Sea Drilling Project, 1977.

779 Phillips, J. D., and Forsyth, D.: Plate Tectonics, Paleomagnetism, and the Opening of the  
780 Atlantic, *Geological Society of America Bulletin*, 83, 1579-1600, 10.1130/0016-  
781 7606(1972)83[1579:ptpato]2.0.co;2, 1972.

782 Pollard, D., and DeConto, R. M.: Hysteresis in Cenozoic Antarctic ice-sheet variations,  
783 *Global and Planetary Change*, 45, 9-21, 2005.

784 Polzin, K. L., Toole, J. M., Ledwell, J. R., and Schmitt, R. W.: Spatial Variability of  
785 Turbulent Mixing in the Abyssal Ocean, *Science*, 276, 93-96,  
786 10.1126/science.276.5309.93, 1997.

787 Roberts, C. D., LeGrande, A. N., and Tripathi, A. K.: Climate sensitivity to Arctic seaway  
788 restriction during the early Paleogene, *Earth and Planetary Science Letters*, 286,  
789 576-585, 10.1016/j.epsl.2009.07.026, 2009.

790 Rosenbloom, N., Shields, C., Brady, E. C., Levis, S., and Yeager, S. G.: Using CCSM3 for  
791 Paleoclimate Applications NATIONAL CENTER FOR ATMOSPHERIC RESEARCH,  
792 2011.

793 Scher, H. D., and Martin, E. E.: Timing and Climatic Consequences of the Opening of  
794 Drake Passage, *Science*, 312, 428-430, 10.1126/science.1120044, 2006.

795 Schlich, R.: Sites 246 and 247, DSDP Deep Sea Drilling Project, 1974.

796 Schubert, G., and Sandwell, D.: Crustal volumes of the continents and of oceanic and  
797 continental submarine plateaus, *Earth & Planetary Science Letters*, 92, 234-246,  
798 1989.

799 Scotese, C. R., and Golonka, J.: Paleogeographic Atlas, PALEOMAP Progress Report 20-  
800 0692, Department of Geology, University of Texas at Arlington, 34, 1992.

801 Sessa, J. A., Ivany, L. C., Schlossnagle, T. H., Samson, S. D., and Schellenberg, S. A.:  
802 The fidelity of oxygen and strontium isotope values from shallow shelf settings:  
803 Implications for temperature and age reconstructions, *Palaeogeography,*  
804 *Palaeoclimatology,* *Palaeoecology*, 342-343, 27-39,  
805 <http://dx.doi.org/10.1016/j.palaeo.2012.04.021>, 2012.

806 Sewall, J. O., Sloan, L. C., Huber, M., and Wing, S.: Climate sensitivity to changes in  
807 land surface characteristics, *Global and Planetary Change*, 26, 445-465, 2000.

808 Sewall, J. O., and Sloan, L. C.: Come a little bit closer: A high-resolution climate study of  
809 the early Paleogene Laramide foreland, *Geology*, 34, 81-84, 10.1130/g22177.1,  
810 2006.

811 Shellito, C. J., Sloan, L. C., and Huber, M.: Climate model sensitivity to atmospheric CO2  
812 levels in the Early-Middle Paleogene, *Palaeogeography, Palaeoclimatology,*  
813 *Palaeoecology*, 193, 113-123, 2003.

814 Shellito, C. J., and Sloan, L. C.: Reconstructing a lost Eocene paradise: Part I. Simulating  
815 the change in global floral distribution at the initial Eocene thermal maximum,  
816 *Global and Planetary Change*, 50, 1-17, 2006a.

817 Shellito, C. J., and Sloan, L. C.: Reconstructing a lost Eocene Paradise, Part II: On the  
818 utility of dynamic global vegetation models in pre-Quaternary climate studies,  
819 *Global and Planetary Change*, 50, 18-32, 2006b.

820 Shellito, C. J., Lamarque, J.-F., and Sloan, L. C.: Early Eocene Arctic climate sensitivity  
821 to pCO2 and basin geography, *Geophys. Res. Lett.*, 36, 10.1029/2009gl037248,  
822 2009.

823 Simmons, H. L., Jayne, S. R., Laurent, L. C. S., and Weaver, A. J.: Tidally driven mixing  
824 in a numerical model of the ocean general circulation, *Ocean Modelling*, 6, 245-  
825 263, [http://dx.doi.org/10.1016/S1463-5003\(03\)00011-8](http://dx.doi.org/10.1016/S1463-5003(03)00011-8), 2004.

826 Sloan, L. C.: Equable climates during the early Eocene; significance of regional  
827 paleogeography for North American climate, *Geology*, 22, 881-884, 1994.

828 Sloan, L. C., and Rea, D. K.: Atmospheric carbon dioxide and early Eocene climate: A  
829 general circulation modeling sensitivity study, *Palaeogeography,*  
830 *Palaeoclimatology, Palaeoecology*, 119, 275-292, 1996.

831 Stein, C. A., and Stein, S.: A model for the global variation in oceanic depth and heat  
832 flow with lithospheric age, *Nature*, 359, 123-129, 1992.

833 Stickley, C. E., Brinkhuis, H., Schellenberg, S. A., Sluijs, A., Röhl, U., Fuller, M., Grauert,  
834 M., Huber, M., Warnaar, J., and Williams, G. L.: Timing and nature of the  
835 deepening of the Tasmanian Gateway, *Paleoceanography*, 19, PA4027,  
836 10.1029/2004pa001022, 2004.

837 Stocker, T., Qin, D., and Plattner, G.: Climate Change 2013: The Physical Science Basis,  
838 Working Group I Contribution to the Fifth Assessment Report of the  
839 Intergovernmental Panel on Climate Change. Summary for Policymakers (IPCC,  
840 2013), 2013.

841 Strömberg, C. A. E.: Evolution of Grasses and Grassland Ecosystems, *Annual Review of*  
842 *Earth and Planetary Sciences*, 39, 517-544, doi:10.1146/annurev-earth-040809-  
843 152402, 2011.

844 Torsvik, T. H., Carlos, D., Mosar, J., Cocks, L. R. M., and Malme, T. N.: Global  
845 reconstructions and North Atlantic paleogeography 440 Ma to recent, *BATLAS—*  
846 *Mid Norway plate reconstruction atlas with global and Atlantic perspectives*, 18-  
847 39, 2002.

848 Utescher, T., and Mosbrugger, V.: Eocene vegetation patterns reconstructed from plant  
849 diversity — A global perspective, *Palaeogeography, Palaeoclimatology,*  
850 *Palaeoecology*, 247, 243-271, 10.1016/j.palaeo.2006.10.022, 2007.

- 851 Vincent, E., Gibson, J. M., and Brun, L.: Paleocene and early Eocene microfacies,  
852 benthonic foraminifera, and paleobathymetry of Deep Sea Drilling Project sites  
853 236 and 237, western Indian Ocean, DSDP Deep Sea Drilling Project, 1974.
- 854 Vinogradov, A. P., SSSR., A. a. n., and geologii, S. U. M.: Atlas of the Lithological-  
855 paleogeographical Maps of the USSR, 1967.
- 856 Whittaker, J. M., Goncharov, A., Williams, S. E., Müller, R. D., and Leitchenkoy, G.:  
857 Global sediment thickness data set updated for the Australian-Antarctic Southern  
858 Ocean, *Geochemistry, Geophysics, Geosystems*, n/a-n/a, 10.1002/ggge.20181,  
859 2013.
- 860 Wilson, D. S., Jamieson, S. S. R., Barrett, P. J., Leitchenkoy, G., Gohl, K., and Larter, R.  
861 D.: Antarctic topography at the Eocene–Oligocene boundary, *Palaeogeography,*  
862 *Palaeoclimatology, Palaeoecology*, 335–336, 24–34,  
863 <http://dx.doi.org/10.1016/j.palaeo.2011.05.028>, 2012.
- 864 Winguth, A., Shellito, C., Shields, C., and Winguth, C.: Climate Response at the  
865 Paleocene–Eocene Thermal Maximum to Greenhouse Gas Forcing—A Model Study  
866 with CCSM3, *Journal of Climate*, 23, 2562–2584, 10.1175/2009jcli3113.1, 2009.
- 867 Wohlfahrt, J., Harrison, S., Braconnot, P., Hewitt, C., Kitoh, A., Mikolajewicz, U., Otto-  
868 Bliesner, B., and Weber, S.: Evaluation of coupled ocean–atmosphere simulations  
869 of the mid-Holocene using palaeovegetation data from the northern hemisphere  
870 extratropics, *Climate Dynamics*, 31, 871–890, 10.1007/s00382-008-0415-5,  
871 2008.
- 872 Wolfe, J. A.: Distribution of major vegetational types during the Tertiary, in: *Geophysical*  
873 *Monograph*, edited by: Sundquist, E. T., and Broecker, W. S., American  
874 Geophysical Union, Washington, DC, 357–375, 1985.
- 875 Wolfe, J. A., Forest, C. E., and Molnar, P.: Paleobotanical evidence of Eocene and  
876 Oligocene paleoaltitudes in midlatitude western North America, *Geological Society*  
877 *of America Bulletin*, 110, 664–678, 10.1130/0016-  
878 7606(1998)110<0664:peoeao>2.3.co;2, 1998.
- 879 Wright, N., Zahirovic, S., Müller, R. D., and Seton, M.: Towards community-driven  
880 paleogeographic reconstructions: integrating open-access paleogeographic and  
881 paleobiology data with plate tectonics, *Biogeosciences*, 10, 1529–1541,  
882 10.5194/bg-10-1529-2013, 2013.
- 883 Zachos, J. C., Röhl, U., Schellenberg, S. A., Sluijs, A., Hodell, D. A., Kelly, D. C.,  
884 Thomas, E., Nicolo, M., Raffi, I., Lourens, L. J., McCarren, H., and Kroon, D.:  
885 Rapid Acidification of the Ocean During the Paleocene-Eocene Thermal Maximum,  
886 *Science*, 308, 1611–1615, 10.1126/science.1109004, 2005.
- 887 Ziegler, A. M., Scotese, C. R., and Barrett, S. F.: Mesozoic and Cenozoic Paleogeographic  
888 Maps, in: *Tidal Friction and the Earth’s Rotation II*, edited by: Brosche, P., and  
889 Sündermann, J., Springer Berlin Heidelberg, 240–252, 1982.
- 890 Ziegler, A. M., Rowley, D. B., Lottes, A. L., Sahagian, D. L., Hulver, M. L., and  
891 Gierlowski, T. C.: Paleogeographic Interpretation: With an Example From the Mid-  
892 Cretaceous, *Annual Review of Earth and Planetary Sciences*, 13, 385–428,  
893 doi:10.1146/annurev.earth.13.050185.002125, 1985.

894

895

Figure 1. Herold et al.

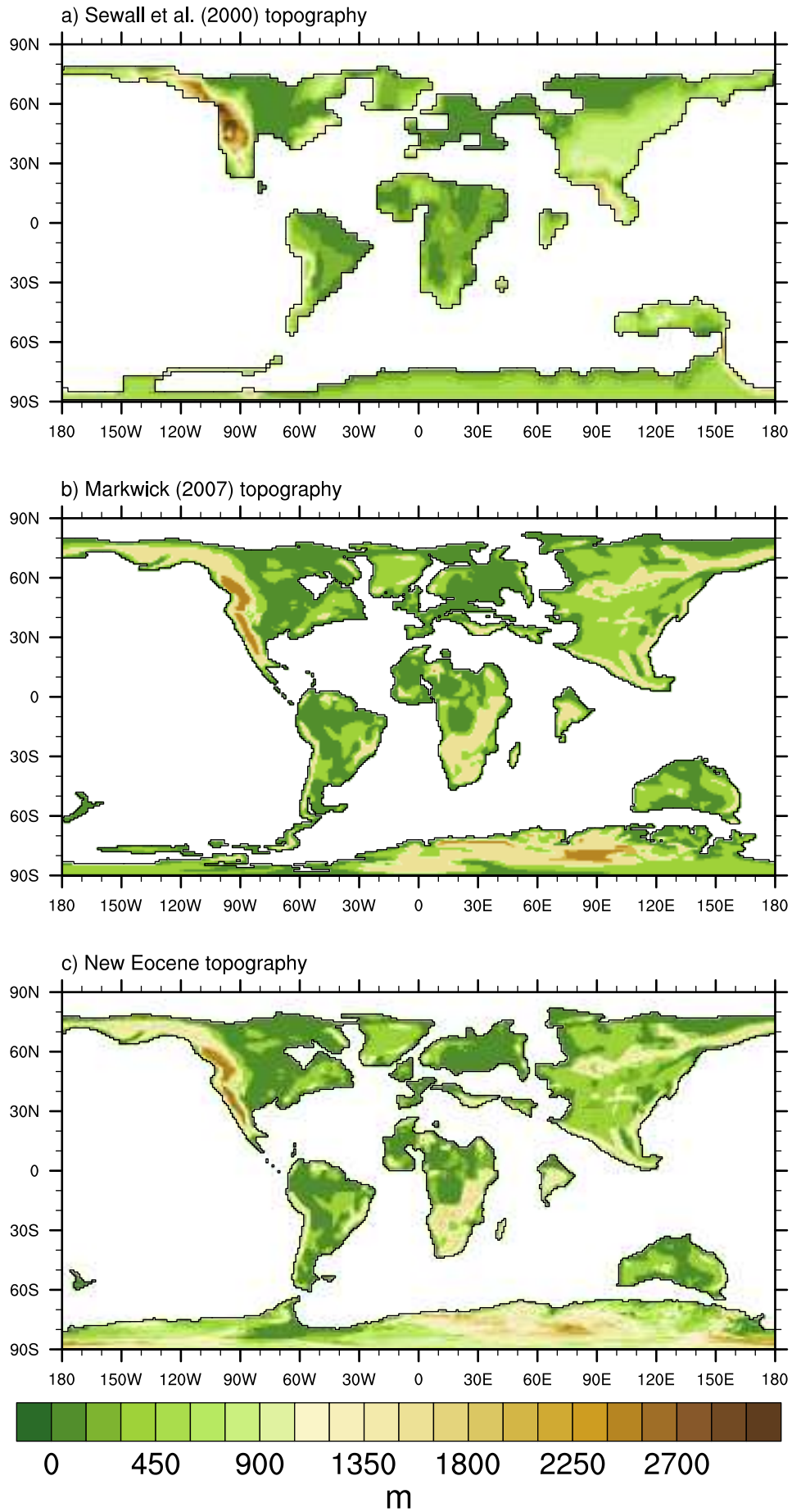


Figure 2 Herold et al.

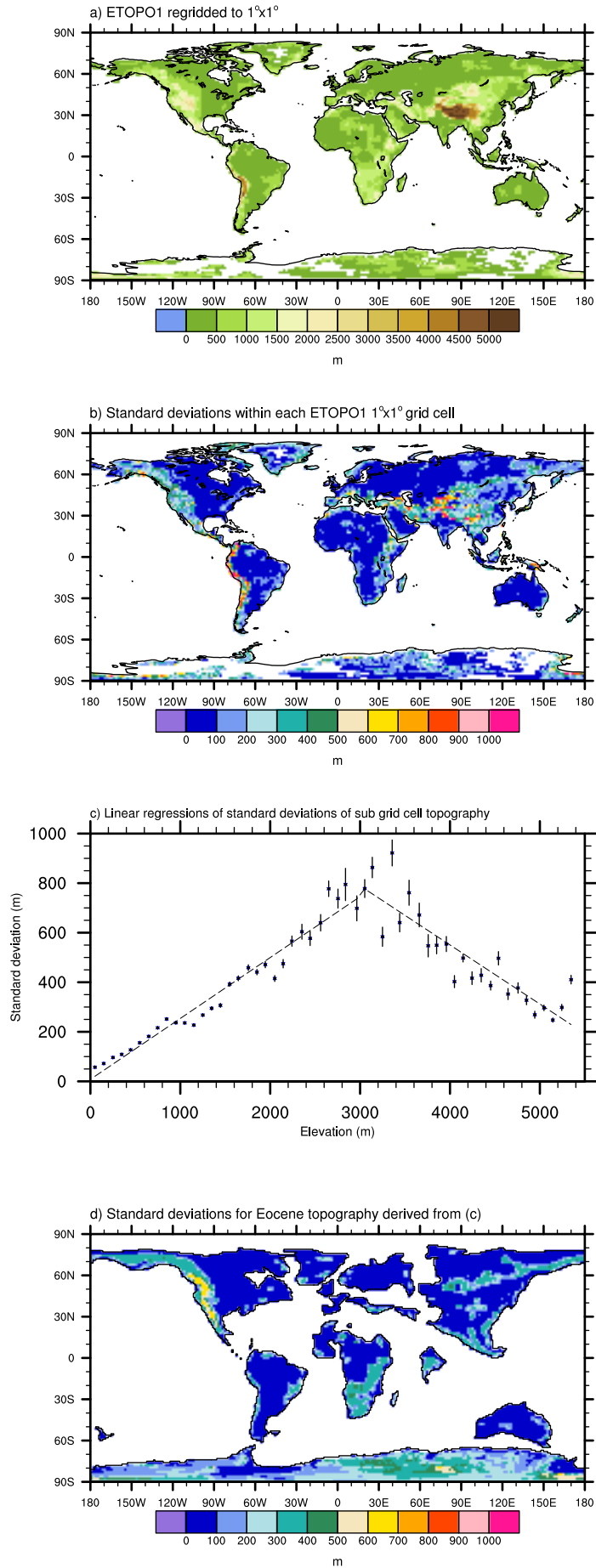


Figure 3. Herold et al.

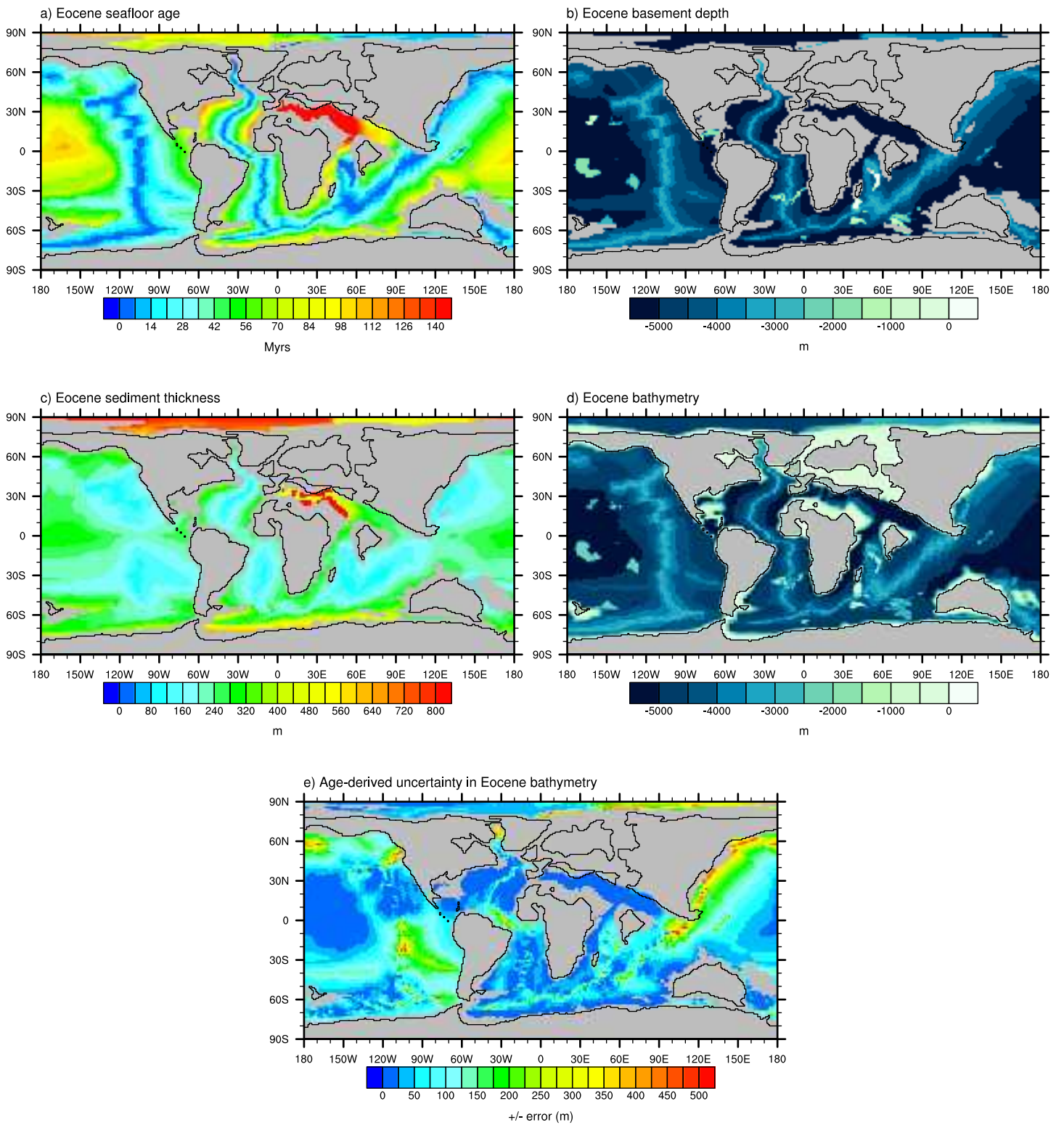
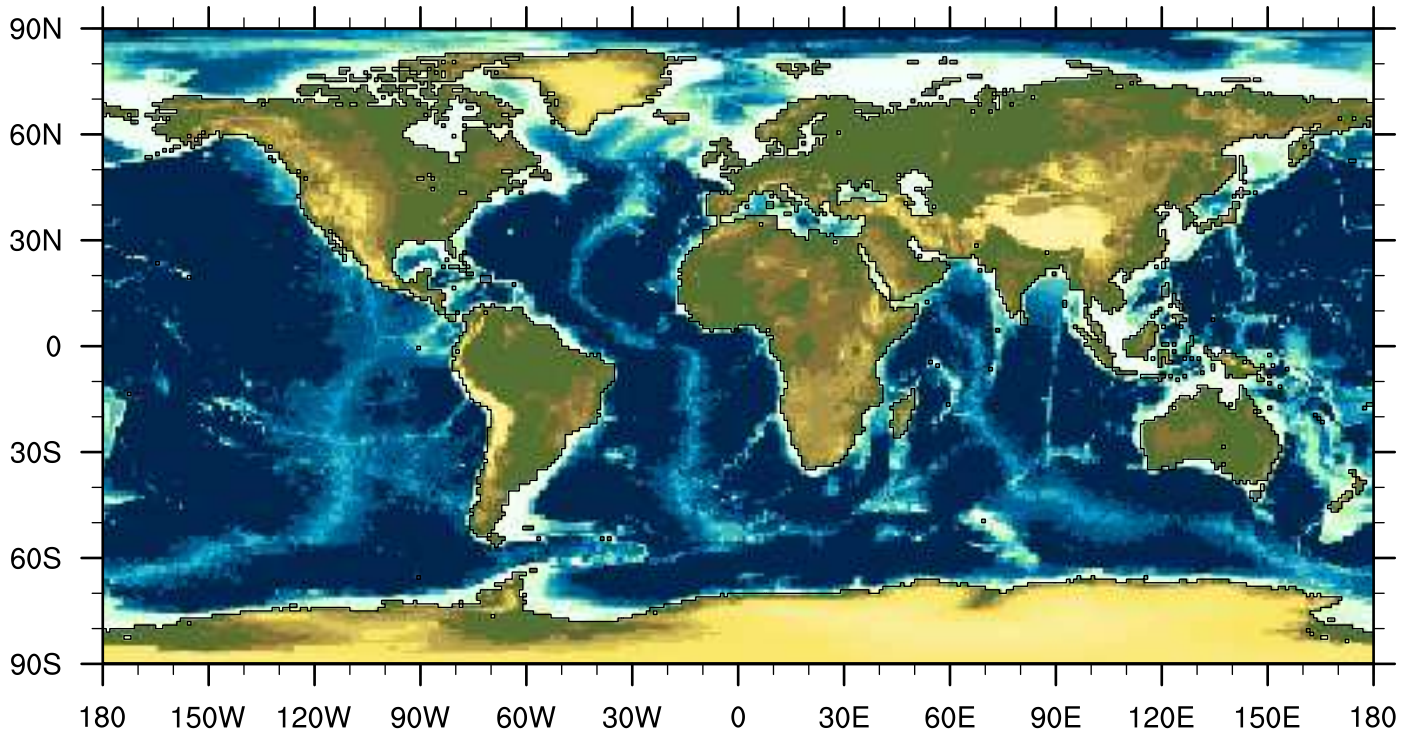


Figure 4. Herold et al.

a) ETOPO1



b) Eocene topography and bathymetry

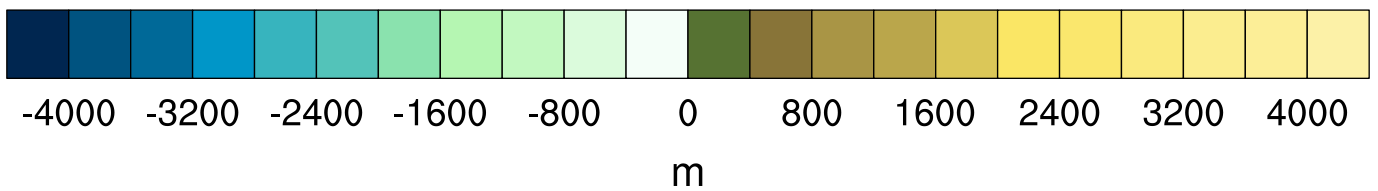
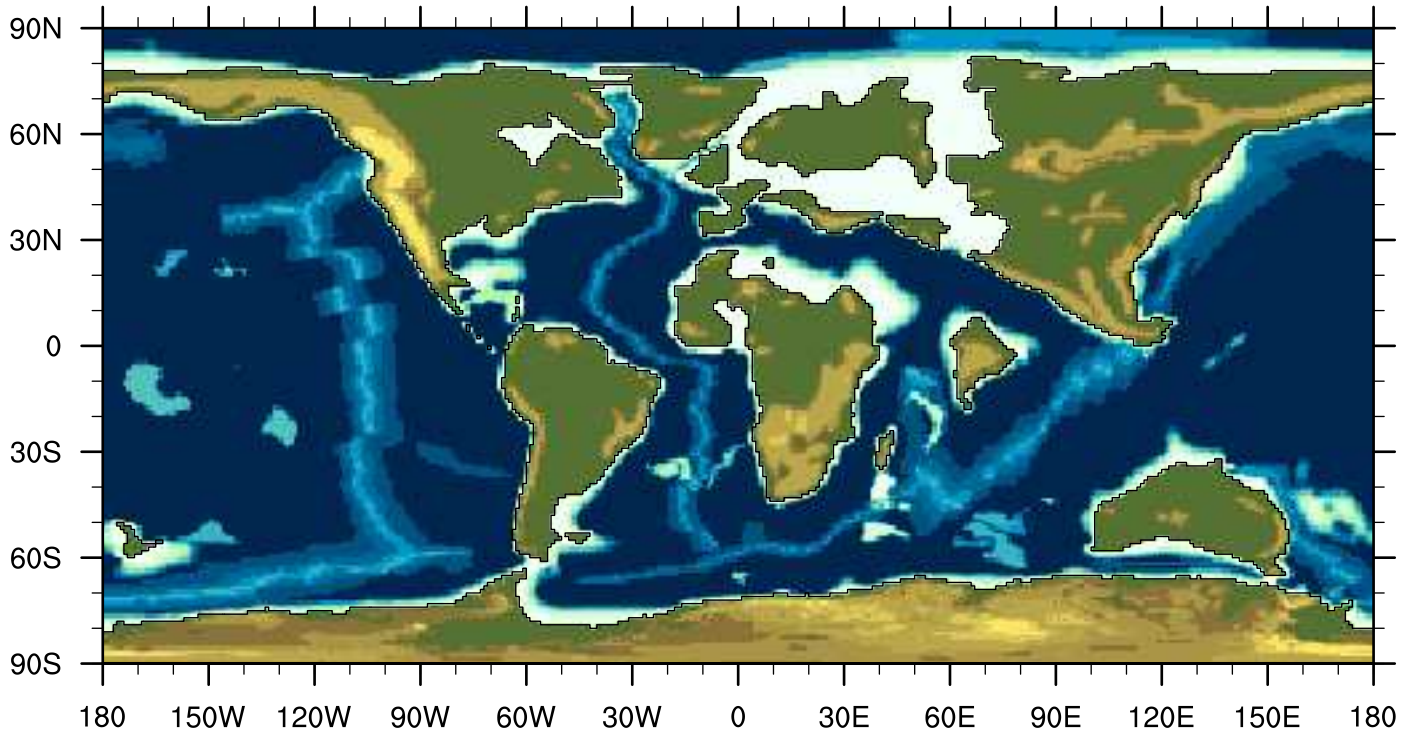


Figure 5. Herold et al.

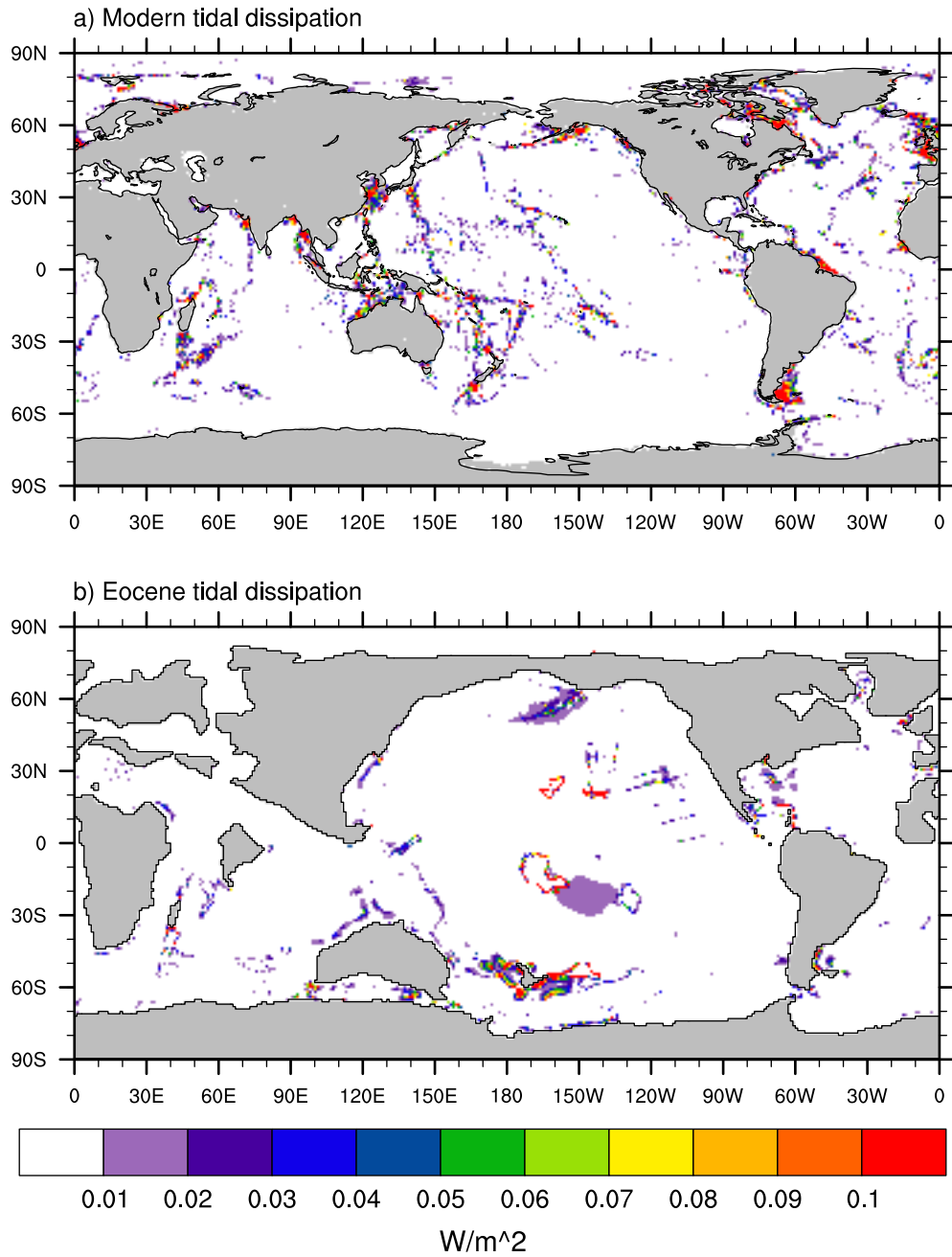




Figure 6. Herold et al.

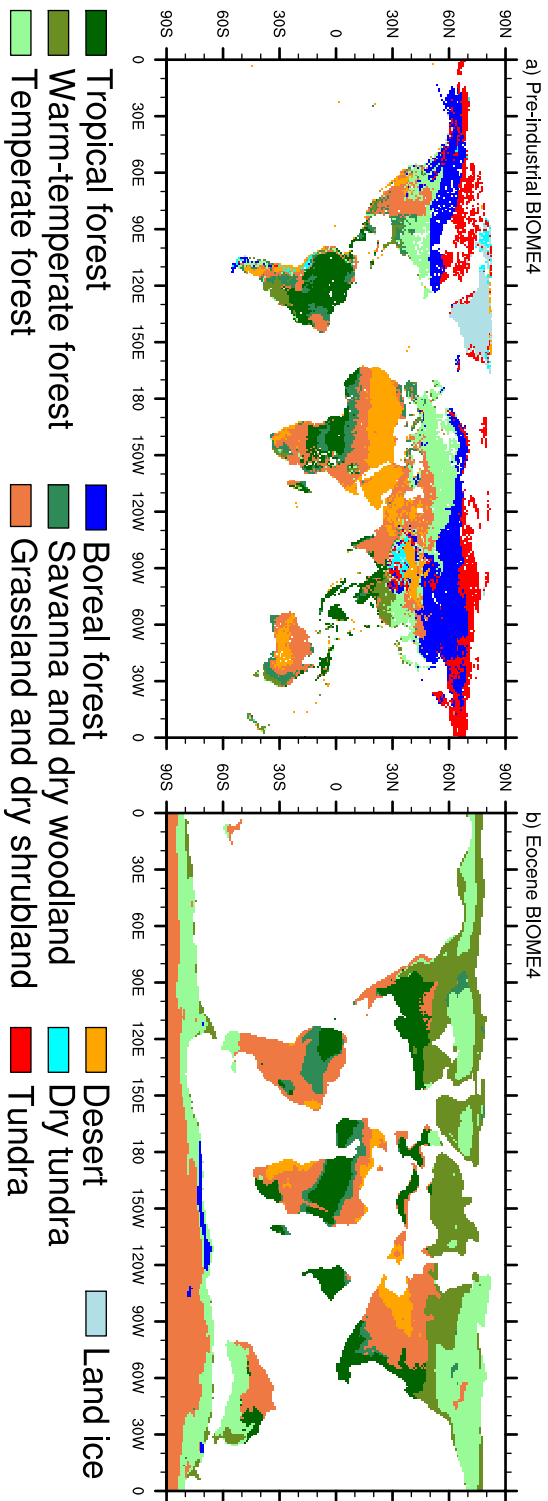


Figure 7. Herold et al.

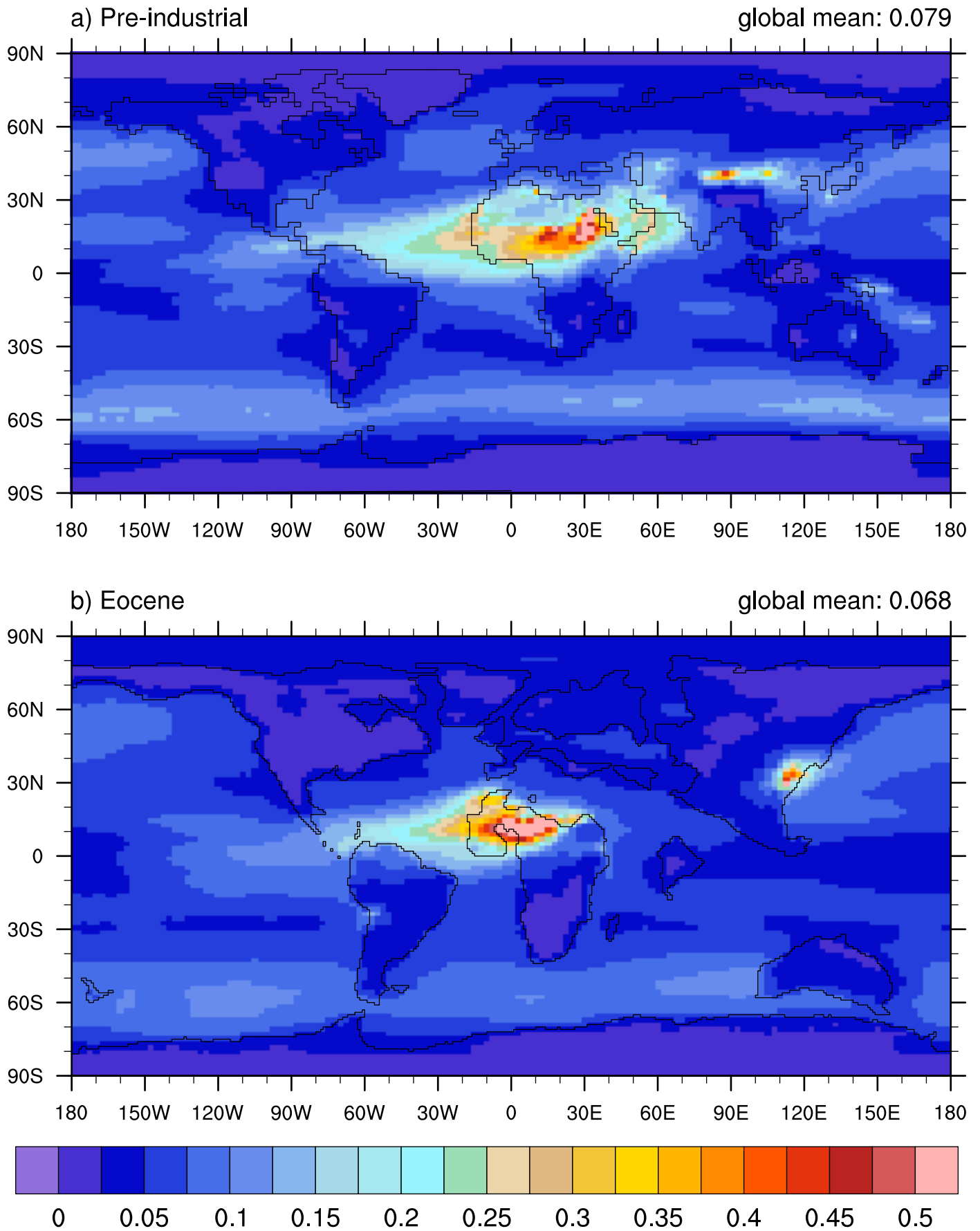


Figure 8. Herold et al.

